Large-Scale Synthesis of Wide Band Gap Semiconductor Nanostructures by Microwave Method

ARTICLE *in* THE JOURNAL OF PHYSICAL CHEMISTRY C · NOVEMBER 2009

Impact Factor: 4.77 · DOI: 10.1021/jp904227n

11 AUTHORS, INCLUDING:

Guodong Wei
Southern University and A&M College
87 PUBLICATIONS **1,001** CITATIONS
SEE PROFILE

Weiping Qin
Jilin University
360 PUBLICATIONS **3,702** CITATIONS
SEE PROFILE

D.M. Zhang
Jilin University
190 PUBLICATIONS **1,405** CITATIONS
SEE PROFILE

Lili Wang
Institute of Atmospheric Physics
162 PUBLICATIONS **2,622** CITATIONS
SEE PROFILE

Large-Scale Synthesis of Wide Band Gap Semiconductor Nanostructures by Microwave Method

Guodong Wei,[†,‡,§] Weiping Qin,[*,†] Wei Han,[*,‡] Weiyou Yang,[§] Fengmei Gao,[§] Guangzhu Jing,[§] Ryongjin Kim,[†] Daisheng Zhang,[†] Kezhi Zheng,[†] Lili Wang,[†] and Ling Liu[†]

State Key Laboratory on Integrated Optoelectronics, College of Electronic Science and Engineering, College of Physics, Jilin University Changchun, 130021, People's Republic of China, and Ningbo University of Technology, Ningbo, 315016, People's Republic of China

Received: May 6, 2009; Revised Manuscript Received: September 9, 2009

Low-dimension semiconductor nanostructures were successfully synthesized by a fast, simple, and low-cost microwave method. By heating raw materials under microwave irradiation and controlled conditions, diverse nanostructures for semiconducting oxides and carbides were synthesized without extra metal catalysts. In this paper, flower-like and net structural oxide and carbide semiconductors in nanoscale have been studied in detail. Structural, morphological, and elemental analysis revealed that the as-synthesized nanostructures were highly pure and structurally uniform. The possible growth mechanisms of these nanostructures were preliminarily discussed. The temperature and the gas-phase supersaturation in their growing processes have important effects on their morphologies. The unique synthesis method may open a new way for the fabrication of self-assembled multidimensional structures, which are expected to find a wide range of important applications in nanodevices and nanocomposites.

Introduction

One-dimension (1D) nanostructures, such as nanowires, nanobelts, nanotubes, and nanocables, have steadily attracted growing attention due to their high aspect, high surface to volume ratios, as well as novel characteristics originating from their morphologies.[1−8] Among the emerging various 1D nanomaterials, wide band gap semiconductor nanostructures, such as ZnO, SnO_2, Ga_2O_3, SiC, etc., have become the focus of intensive research owing to their unique properties and prospective applications in electronic and optic nanodevices.[1,9−15] Over the past years, great efforts have been devoted to the synthesis of these nanomaterials, and various synthesis methods, such as chemical vapor deposition (CVD),[16] carbon thermal reduction,[17] arc discharge,[18] laser ablation,[19] solution hydrothermal,[20,21] and physical evaporation,[22] have been exploited.

Microwave (MW) heating is a promising preparation method that may resolve the problems rising from the conventional synthesis methods.[23,24] In comparison with the conventional vapor-phase synthesis process, due to its fast heating and cooling characters, the MW evaporation−condensation process can save much energy and time and, thus, reduce the cost of final products. In addition, MW heating has many unique properties, such as homogeneous volumetric heating, high reaction rates and selectivity, dramatically reducing reaction time, and high yields of products.[25,26] Up to now, ZnO nanostructures,[27] CNT−SiC composites,[28] and SiC nanowires[23] have been successfully synthesized by using the MW heating method. More recently, our group has reported the synthesis of SiC nanobelts,[29] 6H-SiC nanowires,[30] and SiC/SiO_2 nanochain heterojunctions[31] by the MW method. These results all presented that the MW method was a simple, low-cost, and fast method for large-scale synthesis of wide band gap semiconductor nanostructures. These interesting results inspire us to explore whether we can use the MW heating method for synthesizing various wide band gap semiconductor nanomaterials with self-assembly into multidimensional structure or not.

In this paper, ZnO, SnO_2, Ga_2O_3, SiO_2, and TiC nanowires, ZnO, Ga_2O_3, and TiNC nanobelts, and SiC nanocables (SiC/SiO_2 and SiC/C) have been synthesized without metal catalysts by MW heating raw materials. In addition, some novel nanostructures, such as ZnO and SnO_2 nanoflowers and Zn_2SnO_4 microwires/net, have been also synthesized. Although some of the above-mentioned nanostructures have been synthesized by other methods, the MW heating method has the advantages as simplicity, high quality and high yields, low cost, energy saving, and easy-to-manufacture nanoproducts. The present results can inspire the exploring of the synthesis of semiconductor nanostructure (oxide, carbide, sulfide, and nitride) by the MW method. More importantly, the MW method can be used for the synthesis of multidimensional nanostructure (flower-like structure and netlike matrix structure), which may have novel properties and have potential applications in many technological fields because of the structure−property relationship in nanostructures. It is believed that these studies have an enormous impact on the nanotechnology and the great potential applications in building blocks for nanodevices in the future.

Experimental Details

Description of the Microwave Heating System. The MW heating system is some like a horizontal tube furnace, and the most difference between them is the heating method. A schematic drawing of the MW heating system is shown in Figure 1. The system consists of a MW oven cavity, a SiC susceptor, quartz tubes, a refractory body, etc. The quartz tubes pass through the cavity, and thus the carrier gas can flow in the left end and out at the right end. Here, the gas flow rate can be adjusted by a mass/master flow controller. The refractory cell

* Corresponding authors. E-mail: wpqin@jlu.edu.cn (W.Q.); whan@jlu.edu.cn (W.H.).
† College of Electronic Science and Engineering, Jilin University.
‡ College of Physics, Jilin University.
§ Ningbo University of Technology.

10.1021/jp904227n CCC: $40.75
Published on Web 10/15/2009

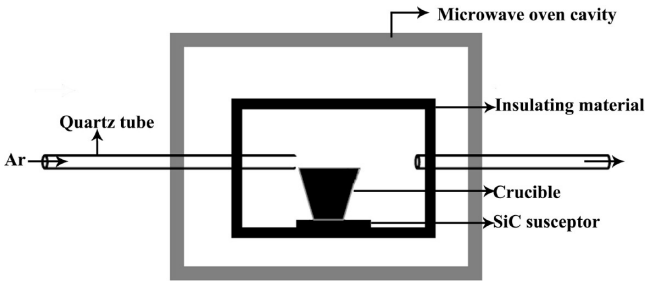

Figure 1. Schematic drawing of the microwave heating system.

inside the MW oven cavity is used as the reaction chamber. The SiC susceptor inside the cell is consisted of several parallel 4H-SiC wafers working as converting MW energy into heat. Due to the high dielectric loss and an excitation/relaxation time according to the changes of MW dipole directions (2.450.000 times a second), SiC wafers efficiently work as a converter of MW energy into heat. The SiC susceptor acts similarly to an electric resistance, from which heat is irradiated and the inner part of the refractory cell is similar to the cavity of the small oven. The temperature of the susceptor could be controlled by adjusting MW power. With use of this MW heating system, the SiC susceptor treated with MW power of 800 W can be heated to high temperatures (in excess of 1300 °C) in just 10 s.

Synthesis. Our synthesis is based on thermal evaporation of raw materials with the above-described MW heating system. It is noted that the morphology and phase structure of the products depend on several experimental parameters, such as MW power, MW heating time, gas flow rate, pressure, source materials, etc. The experimental parameters and properties of the products are listed in Table 1. In a typical synthesis process, raw materials with a certain proportion (Table 1) were encased in an Al_2O_3 crucible and then placed it onto the SiC susceptor. A pure argon stream at a flow rate of 200 mL min^{-1} was introduced into the quartz tube to eliminate air for 10 min. When the furnace started to be heated, the flow rate was turned down at a constant of 10 mL min^{-1}. This flow rate was maintained throughout the entire fabrication process and turned out when the temperature of the products was cooled to ambient temperature. It is noted that most of the products can be synthesized in minutes. After reaction, the products with flocky films were collected from the surface of the raw materials and the inner crucible wall (ZnO, SnO_2, TiC, Ga_2O_3, SiO_2, and Zn_2SnO_4), and SiC nanocables were obtained after being purified by air oxidation at 700 °C for 6 h.

Characterization. The crystal structures and phase purity were examined by X-ray powder diffractometry (XRD, Rigaku RU-200b) using a nickel-filtered Cu Kα radiation ($\lambda = 1.5418$ Å) at room temperature. The morphology and elemental analysis of the obtained products were investigated by scanning electron microscope (FESEM, Hitachi S-4800) equipped with an energy-dispersive spectrometer (EDS). Further detailed structural information of the products was obtained by using a transmission electron microscope (TEM, JEM 2000EX 200 KV). For the TEM observations, the products were dispersed in the alcohol solution with the aid of ultrasonic agitation for 10 min, and then a drop of solution was dropped onto a copper grid covered by porous carbon.

Results and Discussion

ZnO, with a bulk band gap of 3.3 eV, is used as a promising wide band gap semiconductor in various applications, such as chemical sensors, ultraviolet luminescent devices, waveguides, and solar cells.[32,33] Recently, Cheng et al. have successfully synthesized ZnO microtubes and nanowires by the MW method.[27] Therefore, it can be expected that, with the MW method, other nanostructures of ZnO may be also synthesized. First, let us focus on the ZnO nanobelts. After ZnO/C powders were heated by MW for only 30 s, white woollike products were formed on the surface of the raw materials in high yields. SEM observations reveal that the products consist of a large quantity of nanobelts with lengths in the range of several tens to several hundreds of micrometers. Figure 2a obviously reveals that the nanobelts are high bending with homogeneous surfaces. Each nanobelt has a uniform width about several micrometers along its entire length. In addition, no particle has been observed at the ends of the nanobelts, which means that the growth of the nanobelts may be dominated by a vapor−solid (V−S) mechanism. Figure 2b is the SEM image of an individual nanobelt with the thickness of ~40 nm. The width-to-thickness ratios of these nanobelts are in the range of ~5 to 50. A ripple-like contrast observed in the TEM image (Figure 2c) is due to the strain resulting from the bending of the nanobelts. The beltlike morphology is distinct from nanowires. With a well-defined geometry and perfect crystallinity, the nanobelts are likely to be a model material family for a systematic experimental and theoretical understanding in the fundamental electrical, thermal, optical, and ionic transport processes. XRD measurement (Figure 2d) shows that the nanobelts have a high degree of crystallinity. All reflections can be indexed to wurzite-structured ZnO (JCPDS card no. 89-0511) with cell parameters $a = 3.249$ Å and $c = 5.205$ Å. Besides ZnO nanobelts, it is noting that some other interesting ZnO nanostructures can be also synthesized by the MW method. When the MW power was turned up to 800 W and the other experiment parameters

TABLE 1: Summary of the Products Obtained at Optimum Synthesis Parameters[a]

products	raw materials (molar ratio)	microwave power and reaction time	carrier gas
ZnO nanobelts	ZnO/GC = 1:3	640 W, 30 s	Ar
ZnO flowers	ZnO/GC = 1:3	800 W, 30 s	Ar
SnO_2 nanowires	SnO_2/GC = 1:3	800 W, 30 s	Ar
Ga_2O_3 nanowires	Ga_2O_3/GC = 1:3	800 W, 30 s	Ar
Ga_2O_3 nanobelts	Ga_2O_3/GC = 1:3	640 W, 30 s	Ar
Zn_2SnO_4 microwires	ZnO/SnO_2/GC = 2:1:3	800 W, 30 s	Ar
Zn_2SnO_4 nets	ZnO/SnO_2/GC = 1:1:3	640 W, 30 s	Ar
SiO_2 nanowires	Si/SiO_2 = 1:1	640 W, 5 min	Ar
TiC nanowires	TiO_2/charcoal = 1:3	800 W, 20 min	Ar
TiNC nanobelts	TiO_2/charcoal = 1:3	800 W, 20 min	Air
SiC/SiO_2 nanocables	Si/SiO_2/charcoal = 1:2:2	800 W, 30 min	Ar
SiC/C nanocables	Si/SiO_2/charcoal = 1:1:4	800 W, 30 min	Ar

[a] The letters "GC" stand for "graphite + charcoal".

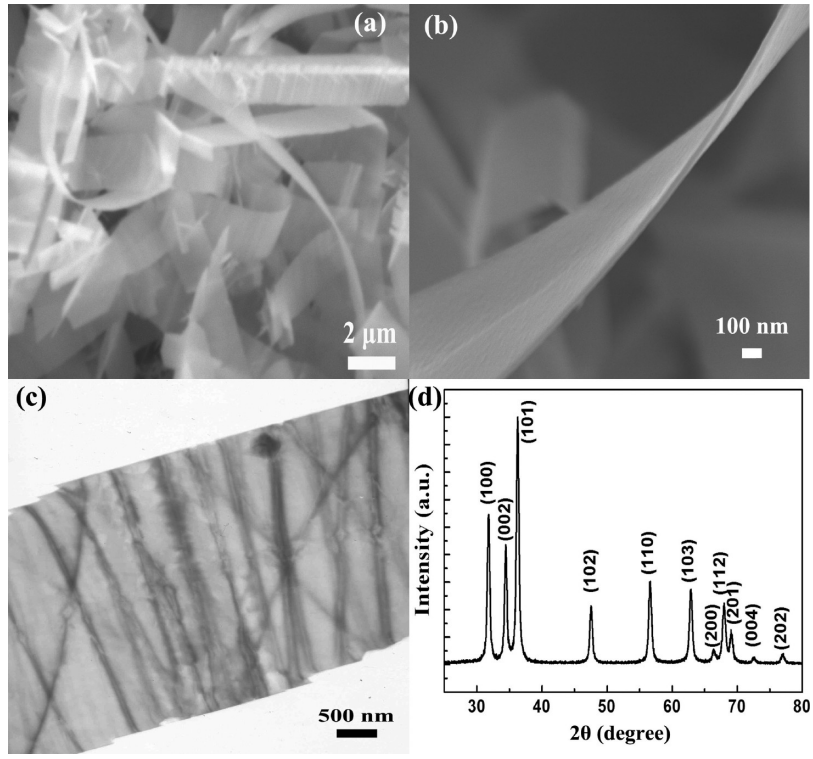

Figure 2. (a) Low-magnification SEM image of as-grown products, showing nanobelts morphology. Panels b and c are typical SEM and TEM images of an individual nanobelt, respectively. (d) XRD pattern of the nanobelts.

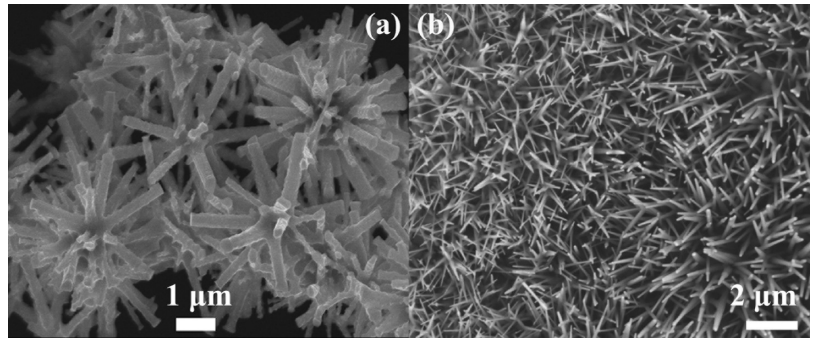

Figure 3. (a) Representative SEM image of ZnO flower structures. (b) A typical SEM image of ZnO nanowire arrays.

remained unchanged, ZnO nanoflowers have been obtained on the surfaces of the starting materials. As displayed in Figure 3a, flower-shaped structures containing rectangle-shaped leaves are exhibited. The typical diameter of one leaf in a flower-shaped structure is about 300−400 nm, whereas the length is always several micrometers, and each leaf's diameter is quite uniform along its length. Each layer contains several leaves, and all the leaves of every layer are rooted at one center. Such many layers consist of the flower-like nanostructures. In addition, ZnO nanowire arrays grown on the inner surface of the crucible could be synthesized in the synthesis process of the above-mentioned ZnO nanostructures (Figure 3b).

SnO_2 is an important semiconducting oxide with a wide band gap of $E_g = 3.6$ eV and has many potential applications.[34,35] Up to date, to the best of our knowledge, unique SnO_2 nanoflowers have not been synthesized by the MW method. At the same time, the growth mechanism of such nanostructure is not clear yet. Therefore, the study of the synthesis and its growth mechanism of such the flower-like structure are an extremely important topic of research in nanoscience about self-assembled multidimensional structure. As shown in Figure 4, parts a and b, the products are composed of diverse SnO_2 flowers with different shapes and sizes of petals, which are about a few to several tens of micrometers in length and about several tens of nanometers in diameter, respectively. A single, very beautiful SnO_2 nanoflower is displayed in the inset of Figure 4a. Like ZnO nanoflowers, the SnO_2 nanowires or nanorods grew homocentrically and self-assembled into nanoflower structures. The selective area electron diffraction (SAED, inset of Figure 4c) pattern reveals that the nanowire is of a single-crystalline nature and grows along the [110] direction. In fact, the whole nanoflower is a single crystal. From the observation of ZnO and SnO_2 nanoflowers, we can infer that the flower-like geometrical morphology is a common structural characteristic for functional oxides with different crystallographic structures, at least for the ones we studied.

Now, a question has raised here why the nanostructure synthesized by the MW method was favorable for forming the nanoflower structure and what exactly the growth mechanism was. Let us take the growth mechanism of the SnO_2 nanoflowers as an example, which is similar with that of the ZnO nanoflowers. The SiC susceptor can be heated to high temperatures

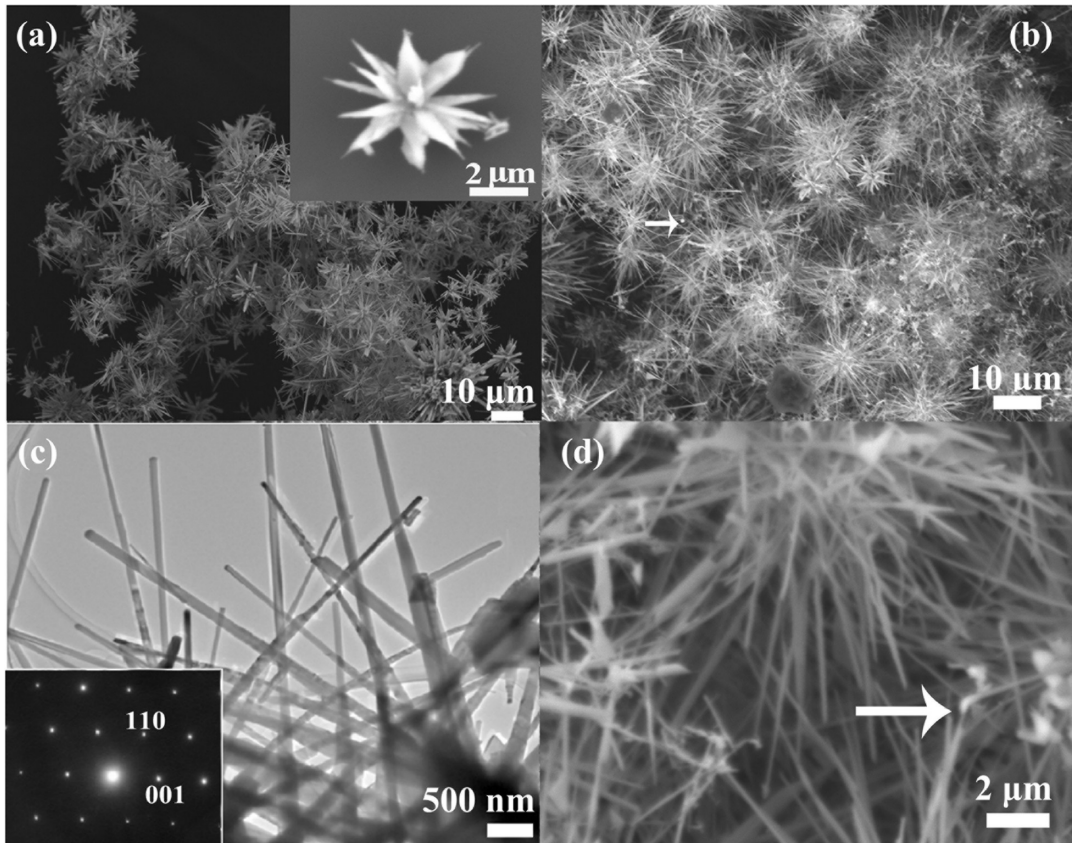

Figure 4. SEM images of SnO_2 nanoflowers: panels a and b are low-magnification SEM images of the nanoflowers. The inset in panel a shows a typical image of an individual nanoflower. (c) A TEM image of SnO_2 nanowires; the inset is the corresponding SAED pattern. (d) Local high-magnification SEM image of panel b, showing the self-assembled flower consisting of nanowires.

(in excess of 1300 °C) in just 10 s in the MW heating system. Thus, three different reactions have been involved in the synthesis process, as illustrated below:

$$SnO_2(s) + C(s) \rightarrow SnO(g) + CO(g) \quad (1)$$

$$2SnO(g) \rightarrow 2Sn(l) + O_2(g) \quad \text{(ref 36)} \quad (2)$$

$$Sn(l) + O_2(g) \rightarrow SnO_2(s) \quad (3)$$

where (s), (l), and (g) stands for solid, liquid, and gas, respectively. In such temperature range, SnO is a gas and Sn is a liquid, respectively. Vapor molecules (SnO) are released from the solid state at a high-temperature zone (the bottom of the crucible) and directly deposit onto a low-temperature zone (on the surface of the reactants). Even more important, a small droplet at the tip of the nanowire (marked in arrow as shown in Figure 4, parts b and d) was found under SEM characterizations. In general, nanostructure grown by vapor−liquid−solid (VLS), a droplet located at the growth front of the nanostructures could be found and acted as the catalytic active site.[37,38] On the basis of the above-mentioned reasons, the growth mechanism of the nanoflowers is dominated by the VLS mechanism. According to the literatures,[37−40] a variety of wirelike and beltlike nanostructures have been produced by the VLS mechanism with introducing metal catalysts. However, in here, sole VLS mechanism is not appropriate for reasonably explaining why the nanowires can self-assemble into nanoflower structures. In addition, due to the MW fast heating ratio, the vapor pressures of the SnO can reach a supersaturated state in a few seconds. Recently, Dai et al. pointed out that the temperature and the supersaturation ratio were two dominant processing factors in controlling the morphology of the products in the VS growth process.[22] Hereby, the supersaturation ratio also plays a very important role in controlling the morphology of the products in the VLS growth process. In the MW heating process, there are excessive metal oxide and metal atom precipitating out in the reaction atmosphere because of the fast heating rate. Sn liquid drops can act as catalysts (self-catalyst function), even though they will be finally oxidized into SnO_2 (marked with an arrow as shown in Figure 4, parts b and d). Once Sn liquid drops form, they will absorb a Sn metal atom from the atmosphere and rapidly grow bigger in a very short time. Due to the Sn metal atom precipitating out in the reaction atmosphere very rapidly, multiple critical nucleations will occur at the liquid−solid interface and continue to grow with each adsorbed molecule, which gives rise to the growth of flower crystals. It is worth pointing out that SnO_2 multiple nucleations grown from Sn liquid droplets may be caused by microwave arcing phenomenon, which can be observed in the experiment process, and relevant plasma environment in the presence of Sn metal under MW irradiation. The growth process of multiple nucleations can be proved as shown in Figure 5, parts a and b. Figure 5a reveals that the nanoflower marked with green color has four petals with all growing from the center site. Figure 5b indicates the clear multiple nucleations marked with the arrow and different petals growing on the same site. From the above analysis, we can conclude that the heating rate, that is, the supersaturation depending on temperature for the given gas, has great effects on the growth of flower-like structures. When the heating rate is at the relatively low, the growth of nanostructure

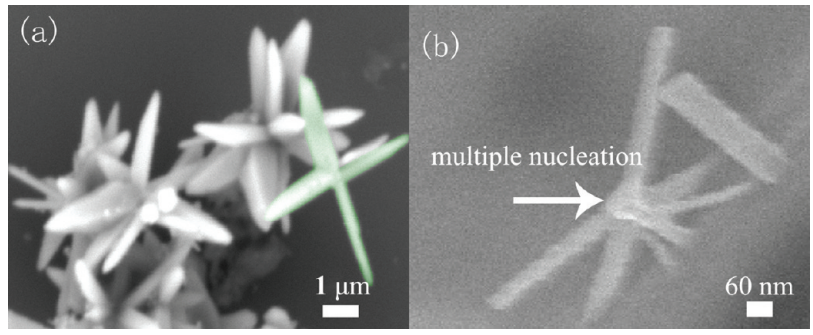

Figure 5. Panels a and b are the SEM images of SnO_2 nanoflowers with their petals growing from the same site, which indicates the presence of the multiple nucleation.

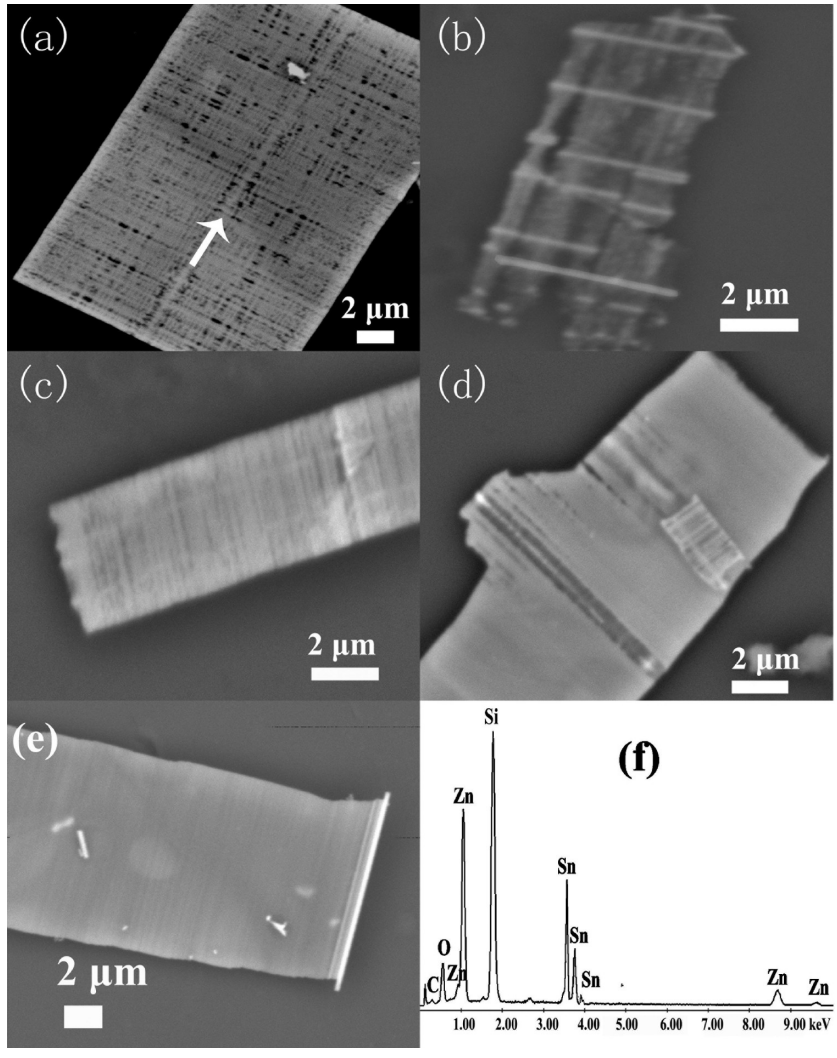

Figure 6. SEM images of the Zn_2SnO_4 matrix. (a) A representative SEM image of the matrix and its corresponding EDS is depicted in panel f. Panels b−e reveal diverse morphology of the net matrix, which indicates the different growth phases from the early to late stages.

by the VLS mechanism takes place at the entire liquid−solid interface and gives rise to solid wires and belts. In other words, the relatively low supersaturation is probably critical for nanowire growth, which should be lower than that required for euhedral crystal growth. Otherwise, two- or three-dimensional growth just like the flower-like structure will occur. This theory could be tested by changing the heating rate in the synthesis of ZnO nanostructures, as shown in Figures 2 and 3. However, it is still an open question how the supersaturation ratio can be responsible for the growth of the nanoflowers. Therefore, the detailed mechanism needs to be further investigated.

When heating the ZnO/SnO_2 mixture powders, we can obtain some very interesting nanostructures. Figure 6 displays representative SEM images of the product. In fact, the product presents a netlike matrix with ribbon morphology. As shown in Figure 6a, two different orientation nanowires are weaving together and constructing a two-dimensional net matrix. It is interesting to note that the angle is about 90° between two different orientations of nanowires. There is a ridgelike nanowire with about 300 nm in diameter in the middle of the matrix, while the rest in the matrix with smaller diameter is nearly perpendicular (parallel) to the ridgelike nanowire. The corre-

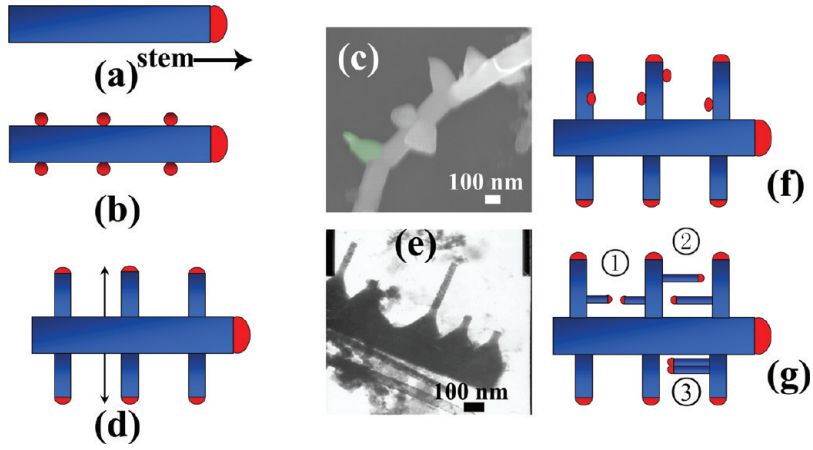

Figure 7. Proposed model for describing the growth mechanism of the matrix. (a) Stem nucleation and growth. Panels b and d are Sn liquid droplets deposition and perpendicular growth on the surface of the stem. The corresponding SEM and TEM images can reveal this process, as shows in panels c and e. Panels f and g are the growth paralleling to the stem.

sponding EDS analysis from Figure 6a reveals that most components of the matrix are elements Zn, Sn, and O, as shown in Figure 6f. The presence of the Si peak comes from the Si substrate used as a support in SEM observations. The atomic ratio of Zn/Sn is about 2:1 and is consistent with stoichiometric Zn_2SnO_4 within experimental error. Figure 6b−e exhibits diverse morphology of such the net matrix, which indicates the different growth phases of the matrix. As shown in Figure 6b, the nanowires parallel to the nanowire marked in green disperse uniformly in the matrix. The rest of them, more like a cluster complex, connect with the above-mentioned nanowires perpendicularly, and the nanowires in two orientations construct the matrix. From Figure 6b, we can infer that this picture may reflect the early growth phase of the matrix and the nanowires prefer to grow in parallel along the width direction of the matrix in the early growth phase. As the growth time goes on, the cluster complex will become high-quality nanowire and the number of holes in the matrix will decrease, as shown in Figure 6, parts c and d. If the growth time is long enough, the holes in the matrix will gradually disappear and the surfaces become smooth. Finally, perfect Zn_2SnO_4 ribbons will be obtained, as shown in Figure 6e.

In order to explore the growth mechanism, another experiment with the heating time of only 10 s was carried out under the same conditions. Figure 7c shows some tips grown on the nanowire, which indicates the growth of the matrix following a VLS mechanism. The similar conclusion can be also obtained from Figure 7e. It can be seen that parallel nanowires are just like grown on the sawtooth substrate. Obviously, Figure 7e reflects the early growth phase of the matrix. Before discussing the growth mechanism of the matrix, we must illuminate the main reactions involved in the synthesis process under MW radiation. It is believed that the thermal reaction of ZnO and SnO with carbon is synchronously carried out among the reaction systems. The reaction mechanism about SnO_2 has been described in eqs 1−3. So here we only give out the reactions of ZnO as the following:

$$ZnO(s) + C(s) \rightarrow Zn(g) + CO(g) \quad (4)$$

$$Zn(g) + O_2(g) \rightarrow ZnO(g) \quad (5)$$

It is pointed out that Zn has low boiling point of ∼906 °C. However, although Sn has low melting point of ∼232 °C, it has high boiling point of ∼2623 °C. Therefore, in the experiment process (actual reaction temperature more than 1000 °C), Zn could be boiled and quickly convert into Zn vapor, while Sn can remain liquid. In other words, as long as the present of metal Zn, it must remain a gas in the whole synthesis process. In the mean time, these Zn vapors could be oxidized to ZnO followed by reaction eq 5. Thus, according to the VLS mechanism, in the growth process of the matrix, there is none but Sn liquid droplet could provide a site for the adsorption of gas like ZnO and SnO vapor to favor the growth of nanowire.

From the experimental results demonstrated above, a simple growth mechanism is proposed for the formation of the matrix, as shown in Figure 7. First, the as-grown Sn liquid drops are the catalyst for the adsorption of ZnO and SnO vapor from the reaction atmosphere to form liquid Sn−Zn−O alloys. With the saturation of Sn, Zn, and O, the Zn_2SnO_4 will be nucleated and the formed Zn_2SnO_4 nanowire (stem) will precipitate on the liquid/solid interface following the VLS mechanism, as shown in Figure 7a. As the stem growth progresses, the new formed Sn liquid drops in the atmosphere would deposit on the newly grown stem (Figure 7, parts b and c) and act as new nucleation sites for the growth of the nanobranches perpendicular to the growth direction of the stem via the VLS mechanism (Figure 7, parts d and e). Once the above-mentioned nanobranches formed, the new nanobranches will grow following the similar growth process, that is, new formed Sn liquid droplets will formed on these nanobranches surface and act as new nucleation sites for the further growth of nanobranches parallel to the growth direction of the stem, resulting in the formation of the net matrix, as shown in Figure 7, parts f and g. The growth process of the parallel nanobranches may have some different processes as following. If two nanowires grow next to each other (area 1 in Figure 7g), they may combine at the tips meet, resulting in a longer nanowire growth. On the other hand, as shown in area 2 in Figure 7g, the branches will keep growing until it meets the nanobranches. If two branches are fairly close in continuous growth, the geometrical coalescence between two neighbored branches will happen and lead to the widening growth of the nanobranches, as shown in area 3 in Figure 7g. As the growth time prolongs, such widening and geometrical coalescence will keep on until all the branches disappeared completely. The detail discussion has been described above in the section of explaining Figure 6a−d. If the growth time is long enough, the matrix with perfect nanoribbon morphology would be achieved, as shown in Figure 6e.

In addition, oxide nanostructures (Ga_2O_3 nanowires and nanobelts, Zn_2SnO_4 microwires, and SiO_2 nanowires) and carbide nanostructures (TiC nanowires, TiNC nanobelts, and SiC nanocables) have also been synthesized by the MW method. The corresponding discussion can been seen in the Supporting Information.

Conclusion

In conclusion, by the MW thermal evaporation synthesis technology, that is, heating raw materials without metal catalysts in a flowing gas at ambient pressure, SnO_2, Ga_2O_3, ZnO, and TiC nanowires, TiNC, Ga_2O_3, and ZnO nanobelts, SiC nanocables, and ZnO and SnO_2 nanoflowers have been obtained. On the basis of SEM, TEM, and EDS analysis, the possible growth mechanisms of the nanoflowers and the net matrix have been discussed. It is believed that the temperature and the supersaturation of the gas in the reaction system mainly affect on the growth of these structures. In addition, the growth of these nanostructures may relate to microwave arcing phenomenon. This method has the advantage of manufacturing wide band gap semiconductors with unique structures in nanoscales. Especially, these multidimensional structures will offer more opportunities for both fundamental research and a crucial object for the design of the nanodevices. Additionally, the unique synthesis method opens a new way for the fabrication of various nanostructures as well as their important applications in nanodevices and nanocomposites.

Acknowledgment. This work was supported by the National High Technology Research and Development Program of China (863 Program Grant Nos. 2007AA068316 and 2009AA03Z309), the National Natural Science Foundation of China (NNSFC) (Grants 10874058 and 50672030), and the Scientific and Technological Planning Project of Jilin Province (Grant No. 20086001).

Supporting Information Available: Additional discussion and SEM images. This material is available free of charge via the Internet at http://pubs.acs.org.

References and Notes

(1) Pan, Z. W.; Dai, Z. R.; Wang, Z. L. *Science* **2001**, *291*, 1947.
(2) Wang, W. Z.; Zeng, B. Q.; Yang, J.; Poudel, B.; Huang, J. Y.; Naughton, M. J.; Ren, Z. F. *Adv. Mater.* **2006**, *18*, 3275.
(3) Qin, W. P.; Wu, C. F.; Qin, G. S.; Zhang, J. S.; Zhao, D. *Phys. Rev. Lett.* **2003**, *90*, 245503.
(4) Qin, Y.; Wang, X. D.; Wang, Z. L. *Nature* **2008**, *451*, 809.
(5) Hu, C. G.; Liu, H.; Dong, W. T.; Zhang, Y. Y.; Bao, G.; Lao, C. S.; Wang, Z. L. *Adv. Mater.* **2007**, *19*, 470.
(6) Mieszawska, A. J.; Jalilian, R.; Sumanasekera, G. U.; Zamborini, F. P. *Small* **2007**, *3*, 722.
(7) Huang, Y.; Duan, X. F.; Cui, Y.; Lauhon, L. J.; Kim, K. H.; Lieber, C. M. *Science* **2001**, *294*, 1313.
(8) Zhang, Y. J.; Wang, N. L.; Gao, S. P.; He, R. R.; Miao, S.; Liu, J.; Zhu, J.; Zhang, X. *Chem. Mater.* **2002**, *14*, 3564.
(9) Zuniga-Perez, J.; Rahm, A.; Czekalla, C.; Lenzner, J.; Lorenz, M.; Grundmann, M. *Nanotechnology* **2007**, *18*, 195303.
(10) Cai, K. F.; Lei, Q.; Zhang, A. X. *J. Nanosci. Nanotechnol.* **2007**, *7*, 580.
(11) Kim, H. W.; Kim, N. H. *Acta Phys. Pol., A* **2005**, *107*, 346.
(12) Taguchi, T.; Yamamoto, H.; Shamoto, S. I. *J. Phys. Chem. C* **2007**, *111*, 18888.
(13) Wang, G. X.; Park, J.; Kong, X. Y.; Wilson, P. R.; Chen, Z. X.; Ahn, J. H. *Cryst. Growth Des.* **2008**, *8*, 1940.
(14) Qi, S. R.; Huang, X. T.; Gan, Z. W.; Ding, X. X.; Cheng, Y. *J. Cryst. Growth* **2000**, *219*, 485.
(15) Li, Y. B.; Bando, Y.; Golberg, D.; Kurashima, K. *Appl. Phys. Lett.* **2002**, *81*, 5048.
(16) Ying, P. Z.; Ni, Z. F.; Xiu, W. J.; Jia, L. J.; Luo, Y. *Chin. Phys. Lett.* **2006**, *23*, 1026.
(17) Feng, Y.; Wang, H. J.; Jin, Z. H. *Inorg. Mater.* **2007**, *22*, 418.
(18) Li, Z. J.; Shen, Z. Q.; Wang, F.; He, L. L. *J. Mater. Sci. Technol.* **2006**, *22*, 113.
(19) Nichols, W. T.; Keto, J. W.; Henneke, D. E.; Brock, J. R.; Malyavanatham, G.; Becker, M. F.; Glicksman, H. D. *Appl. Phys. Lett.* **2001**, *78*, 1128.
(20) Lu, C. H.; Qi, L. M.; Yang, J. H.; Tang, L.; Zhang, D. Y.; Ma, J. M. *Chem. Commun.* **2006**, 3551.
(21) Chang, M.; Chung, C. C.; Deka, J. R.; Lin, C. H.; Chung, T. W. *Nanotechnology* **2008**, *19*, 025710.
(22) Dai, Z. R.; Pan, Z. W.; Wang, Z. L. *Adv. Funct. Mater.* **2003**, *13*, 9.
(23) Sundaresan, S. G.; Davydov, A. V.; Vaudin, M. D.; Levin, I.; Maslar, J. E.; Tian, Y. L.; Rao, M. V. *Chem. Mater.* **2007**, *19*, 5531.
(24) Cerneaux, S.; Xiong, X. Y.; Simon, G. P.; Cheng, Y. B.; Spiccia, L. *Nanotechnology* **2007**, *18*, 055708.
(25) Liu, F. K.; Huang, P. W.; Chang, Y. C.; Ko, C. J.; Ko, F. H.; Chu, T. C. *J. Cryst. Growth* **2005**, *273*, 439.
(26) Cho, S.; Jung, S. H.; Lee, K. H. *J. Phys. Chem. C* **2008**, *112*, 12769.
(27) Cheng, H. B.; Cheng, J. P.; Zhang, Y. J.; Wang, Q. M. *J. Cryst. Growth* **2007**, *299*, 34.
(28) Wang, Y.; Iqbal, Z.; Mitra, S. *Carbon* **2006**, *44*, 2804.
(29) Wei, G. D.; Qin, W. P.; Kim, R. J.; Sun, J. B.; Zhu, P. F.; Wang, G. F.; Wang, L. L.; Zhang, D. S.; Zheng, K. Z. *Chem. Phys. Lett.* **2008**, *461*, 242.
(30) Wei, G. D.; Qin, W. P.; Wang, G. F.; Sun, J. B.; Lin, J. J.; Kim, R. J.; Zhang, D. S.; Zheng, K. Z. *J. Phys. D: Appl. Phys.* **2008**, *41*, 235102.
(31) Wei, G. D.; Qin, W. P.; Zheng, K. Z.; Zhang, D. S.; Sun, J. B.; Lin, J. J.; Kim, R. J.; Wang, G. F.; Zhu, P. F.; Wang, L. L. *Cryst. Growth Des.* **2009**, *9*, 1431.
(32) Mönch, W. *Appl. Phys. Lett.* **2005**, *86*, 162101.
(33) Lao, J. Y.; Huang, J. Y.; Wang, D. Z.; Ren, Z. F. *Nano Lett.* **2003**, *3*, 235.
(34) Wang, W. W.; Zhu, Y. J.; Yang, L. X. *Adv. Funct. Mater.* **2007**, *17*, 59.
(35) Chiu, H. C.; Yeh, C. S. *J. Phys. Chem. C* **2007**, *111*, 7256.
(36) Wang, Z.; Pan, Z. *Appl. Opt.* **1972**, *11*, 533.
(37) Moore, D.; Morber, J. R.; Snyder, R. L.; Wang, Z. L. *J. Phys. Chem. C* **2008**, *112*, 2895.
(38) Lew, K. K.; Pan, L.; Dickey, E. C.; Redwing, J. M. *Adv. Mater.* **2003**, *15*, 2073.
(39) Yang, W.; Miao, H.; Xie, Z.; Zhang, L.; An, L. *Chem. Phys. Lett.* **2004**, *383*, 441.
(40) Lan, Z. H.; Liang, C. H.; Hsu, C. W.; Wu, C. T.; Lin, H. M.; Dhara, S.; Chen, K. H.; Chen, L. C.; Chen, C. C. *Adv. Funct. Mater.* **2004**, *14*, 233.

JP904227N